Biomaterials 34 (2013) 8860–8868

Contents lists available at ScienceDirect

Biomaterials

journal homepage: www.elsevier.com/locate/biomaterials

Rapid tissue engineering of biomimetic human corneal limbal crypts with 3D niche architecture

Hannah J. Levis [a,*], Isobel Massie [a], Marc A. Dziasko [a], Andreas Kaasi [b], Julie T. Daniels [a]

[a] Department of Ocular Biology and Therapeutics, UCL Institute of Ophthalmology, 11-43 Bath Street, London EC1V 9EL, UK
[b] TAP Biosystems, York Way, Royston, Hertfordshire SG8 5WY, UK

ARTICLE INFO

Article history:
Received 10 July 2013
Accepted 1 August 2013
Available online 19 August 2013

Keywords:
Cornea
Collagen
Biomimetic material
Bioengineered limbal crypt
Limbal stem cell niche
Ophthalmology

ABSTRACT

Limbal epithelial stem cells are responsible for the maintenance of the human corneal epithelium and these cells reside in a specialised stem cell niche. They are located at the base of limbal crypts, in a physically protected microenvironment in close proximity to a variety of neighbouring niche cells. Design and recreation of elements of various stem cell niches have allowed researchers to simplify aspects of these complex microenvironments for further study *in vitro*. We have developed a method to rapidly and reproducibly create bioengineered limbal crypts (BLCs) in a collagen construct using a simple one-step method. Liquid is removed from collagen hydrogels using hydrophilic porous absorbers (HPAs) that have custom moulded micro-ridges on the base. The resulting topography on the surface of the thin collagen constructs resembles the dimensions of the stromal crypts of the human limbus. Human limbal epithelial cells seeded onto the surface of the constructs populate these BLCs and form numerous layers with a high proportion of the cells lining the crypts expressing putative stem cell marker, p63α. The HPAs are produced using a moulding process that is flexible and can be adapted depending on the requirements of the end user. Creation of defined topographical features using this process could be applicable to numerous tissue-engineering applications where varied 3-dimensional niche architectures are required.

1. Introduction

The cornea is the transparent window at the front of the eye and the outermost corneal epithelial layer undergoes constant regeneration throughout life. A population of limbal epithelial stem cells (LESCs), morphologically small cells with a high nucleus to cytoplasm (N/C) ratio, are thought to be responsible for the maintenance of this epithelium both in healthy homeostasis and after injury, a concept first proposed by Davanger and Everson [1]. Destruction or damage to this population of stem cells can lead to LESC deficiency and consequent absence of an intact epithelial layer, conjunctival ingrowth and vascularisation, chronic inflammation and impaired vision [2]. Many other organs in the adult body also possess a mechanism to replace cells lost through natural wear and tear or injury, which requires a life-long reservoir of stem cells that retain the ability to self-renew. Given the importance of these cells, it is perhaps unsurprising that they are often found safely hidden away in physically protective environments. These stem cell niches, first described by Schofield in 1978 [3], are frequently characterised by the presence of a diverse array of accessory cell types, which contribute to the specialised extracellular matrix and secreted factor milieu. Examples of these niche environments include the bulge of the hair follicle, the crypt of an intestinal villus, the rete ridges of the epidermis of the skin or the canals of Hering in the liver [4,5], where stem cells are typically located in physically protected positions surrounded by supporting mesenchymal cells.

The LESC stem cell population also resides in a specialised, physically protective niche at the limbus, the vascularised border between the cornea and the conjunctiva. Extensive characterisation of the specific microenvironment, including differential expression of extracellular matrix components and growth factors in the limbal niche has been completed and is well reviewed by Schlötzer-Schrehardt and Kruse [6]. Using advanced imaging techniques, our group has previously identified unique niche structures that house these cells, such as the limbal crypts (LCs) and focal stromal projections (FSPs) [7]. The stromal tissue that surrounds the LCs is highly cellular with a distinct vascular supply that is closely associated with the small epithelial cells at the base of the crypts. The LCs and FSPs are not uniformly distributed around the corneal

* Corresponding author. Tel.: +44 (0) 207 608 6996; fax: +44 (0) 207 608 6887.
E-mail addresses: h.levis@ucl.ac.uk, hannah.levis@hotmail.co.uk (H.J. Levis).

0142-9612/$ – see front matter © 2013 Elsevier Ltd. All rights reserved.
http://dx.doi.org/10.1016/j.biomaterials.2013.08.002

circumference but are predominantly located in the superior and inferior corneal limbal quadrants, areas that are afforded extra protection from damaging ultraviolet light by the eyelids [8]. One major advantage of studying the human limbal niche is that it is readily accessible allowing detection of the LCs and FSPs using *in vivo* confocal microscopy in healthy human volunteers. In studies in patients with LESC deficiency, no LCs or FSPs could be detected [7], emphasising the importance of these structures to maintenance of normal LESC function. Confocal imaging of limbal tissue has revealed a close spatial relationship between basal LESCs of the LCs and stromal cells [9], much like the mesenchymal cells of the haematopoietic stem cell niche in the bone marrow [10]. In a tissue-engineered model of the central cornea, we have previously demonstrated how the presence of these stromal cells in close proximity to an overlying epithelial layer positively affects the organisation of that epithelium [11].

Considerable progress has been made in the design of engineered, completely artificial niches that allow researchers to simplify elements of complex stem cell niches for further study *in vitro* (for review see Ref. [12]). Elements of the niche that have been targeted for reproduction have included integral membrane proteins on support cells, localized secreted ECM components and soluble proteins such as growth factors and cytokines. In addition, conventional attempts to recreate aspects of the stem cell niche have commonly focussed on two-dimensional microenvironmental configurations, such as growth on nano-scale topography on tissue culture plastic. More recently, bioprinting technologies have been employed in this field. Creation of spatially defined patterns of immobilized proteins using inkjet-printing technology instructs progenitor cells to differentiate into disparate cells types depending on whether on-pattern or off-pattern [13]. Albrecht et al. have taken this one step further by precisely organising cells in 3-dimensional (3-D) microenvironments using electropatterning within hydrogels [14] and Nelson and Tien highlight the importance of mimicry of the microscale geometry of niche extracellular matrix for tissue engineering [15].

We have previously reported production of a model of the central cornea using plastic compressed collagen containing limbal fibroblasts as a substrate for epithelial cell growth [11] and have further developed this process to increase robustness and allow scale-up in production of engineered tissues [16]. Since then, the process has been further refined taking into consideration the requirements for compliance for production in good manufacturing practice (GMP) facilities. The new process for production is referred to as **R**eal **A**rchitecture **F**or 3D **T**issue or RAFT™. We believe that the unique physical LC structures identified in the limbus are a major contributing element to the LESC niche. We aim to create a model of the LESC niche with increased biomimicry, by engineering crypts into the surface of stromal fibroblast-containing RAFT constructs using a novel, rapid, reproducible and tunable process. We aim to show that these bioengineered limbal crypts (BLCs) are stable in culture and that human limbal epithelial (HLE) cells and cells with limbal stem cell characteristics consistently populate these crypts.

2. Materials and methods

2.1. Donor tissue

Cadaveric donor corneal rims and whole corneas with appropriate research consent were obtained from Moorfields Lions Eye Bank (London, UK) and Florida Lions Eye Bank (Miami, FL, US). Ethical permission was obtained from the Research Ethics committee (UK) (Ref No. 10/H0106/57). Corneas were stored at 4 °C in Optisol (Chiron Ophthalmics Inc. Irvine, California) after enucleation and prior to fixation or HLE cell and human limbal fibroblast (HLF) isolation.

2.2. Isolation and culture of human limbal epithelial cells

Human donor corneal rims were quartered and placed in a solution of 1.2 U ml^{-1} dispase II (Roche Diagnostics, GmbH, Manheim, Germany) for 2 h at 37 °C. HLE cells were isolated by scraping the limbus with forceps and collecting the liberated cells in corneal epithelial cell medium (CECM). CECM contained DMEM:F12 basal medium (3:1), 10% foetal bovine serum (FBS), 1% antibiotic-antimycotic, epidermal growth factor (EGF, 10 ng/ml; Life Technologies, Paisley, UK), hydrocortisone (0.4 mg/ml), insulin (5 mg/ml), adenine (0.18 mM), transferrin (5 mg/ml), T3 (2 nM) and cholera toxin (0.1 nM; Sigma–Aldrich, Dorset, UK). A single cell suspension of HLE cells was seeded onto a feeder layer of 3T3-J2 cells that had been growth arrested with mitomycin C (Movianto, Stuttgart, DE) for 2 h. Cells were maintained in a 5% CO_2 humidified incubator at 37 °C. Culture medium was changed 3 times a week and cells harvested when 80% confluent using 0.5% trypsin-EDTA (Life Technologies, Paisley, UK).

2.3. Culture of HCE-T cell line

The SV-40 immortalized human corneal epithelial cell line, HCE-T, was cultured in HCE-T medium containing DMEM:Ham's F12 (1:1), 5% FBS, insulin (5 μg/ml), cholera toxin (0.1 μg/ml) and EGF (10 ng/ml). The cell line exhibits a cobblestone appearance similar to normal corneal epithelial cells in culture [17]. HCE-T cells were used to optimize cell seeding experiments on surfaces with varied topography.

2.4. Isolation and culture of human limbal fibroblasts

After isolation of HLE cells, the remaining stromal pieces were trimmed to remove excess sclera and central cornea and placed into a solution of 2 mg/ml collagenase (Life Technologies, Paisley, UK) overnight at 37 °C. The isolated cells were then cultured in HLF medium containing DMEM-Glutamax, 10% FBS and 1% antibiotic-antimycotic (Life Technologies, Paisley, UK). Cells were maintained in a 5% CO_2 humidified incubator at 37 °C. Fibroblasts were expanded and harvested using 0.05% trypsin-EDTA and used in experiments up to passage six.

2.5. Preparation of collagen solution

A collagen solution was prepared by mixing 80% vol/vol sterile rat tail type I collagen (2 mg ml^{-1}; First Link, Birmingham, UK) with 10% vol/vol 10× Minimum Essential Medium (Life Technologies, Paisley, UK). After neutralisation with 5 M sodium hydroxide the final 10% vol/vol HLF medium containing 80,000 HLF/ml of final volume was added or HLF medium alone if acellular RAFT constructs were required.

2.6. Preparation of RAFT constructs

A volume of 2.4 ml of collagen solution (acellular or cellular) was added to the wells of 24 well plates (Greiner Bio-One, Stonehouse, UK). The well plate was placed on a plate heater (TAP Biosystems, Royston, UK) set to 37 °C for 30 min to allow the collagen solution to form a hydrogel. While still on the plate heater, 24-well hydrophilic porous absorbers (HPAs) or ridged HPAs (RHPAs) (TAP Biosystems, Royston, UK) were applied to the surface of the hydrogels. The RAFT absorption process was carried out for 15 min and the majority of the liquid in the collagen hydrogels was removed gently by capillary wicking. The absorbers were then removed and 500 μl of HLF medium was added to each well until HLE cell seeding. Subsequently, HLF medium was removed and 560,000 HLE cells were seeded onto the surface of the constructs in CECM without EGF and cells were allowed to adhere overnight before addition of EGF. Cellular RAFT constructs were maintained at 37 °C with 5% CO_2 in air in submerged culture for 14 days and then placed at the air-liquid interface using 6 well plate cell culture inserts (Millipore, West Lothian, UK) to allow stratification for a further 7 days. When using HCE-T cells, 580,000 cells were seeded on the surface of the constructs in HCE-T medium and maintained in submerged culture for 7 days before airlifting for a further 7 days.

2.7. Thickness measurements of RAFT constructs

The thickness of representative RAFT constructs made using HPAs and RHPAs was measured using optical coherence tomography (OCT) with an anterior segment lens (Spectralis, Heidelberg Engineering, Hemel Hempstead, UK). Constructs were

Table 1
Primary antibody dilution and supply details.

Antibody	Cat#	Concentration	Supplier
Cytokeratin 3	CBL218	1:500	Millipore
p63α	4892	1:100	Cell Signalling Technology
Pax6	PRB-278P	1:100	Covance
Ki67	AB9260	1:100	Millipore

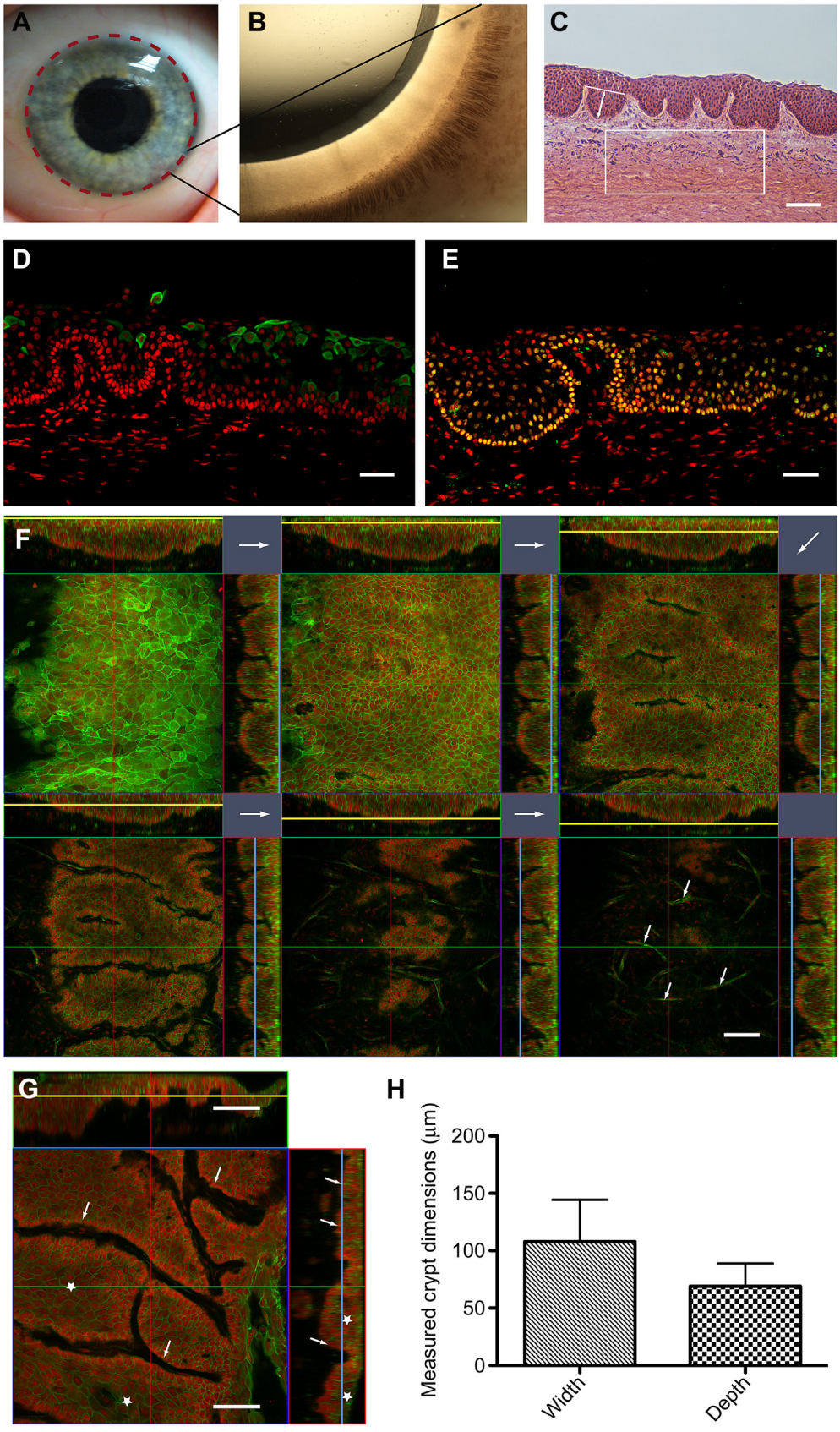

Fig. 1. The human limbal stem cell niche. A) The location of the limbus on the human ocular surface (dashed line). B) Highly pigmented Palisades of Vogt visible in the human limbus. C) H and E stained tangential section of the human limbus showing the LCs. Box indicates a representative area of 0.1 mm^2 of limbal stroma. White line indicates example of LC width measurements and arrowed line LC depth measurements. D) CK3 and E) p63α (green) stained cryosections of human LCs counterstained with PI (red). F) Series of orthogonal confocal images through human LCs stained with phalloidin (green) and PI (red). Yellow lines indicate Z-stack position on *X*-axis and blue lines on *Y*-axis. Large arrows

maintained in culture with HLEs on the surface and HLFs within the construct for 3 weeks. Thickness measurements were taken at 3 positions along the length of 5 scanning positions for each of the 3 replicates. Values are expressed as mean ± standard deviation (SD) and a Student's *T*-test was used to determine significance ($p < 0.05$) using GraphPad Prism software.

2.8. Immunochemistry of cryosections of human limbal tissue

Human limbal tissue pieces were embedded in OCT compound (Tissue-Tek; Sakura, Alphen aan den Rijn, Netherlands) and flash frozen in liquid nitrogen. Tangential and radial sections (7 μm) were cut on a cryostat and mounted onto superfrost plus slides (VWR International, West Sussex, UK). Sections were stored at −80 °C until required, at which time they were fixed with either 100% ice-cold methanol at −20 °C or 4% paraformaldehyde (PFA) at room temperature (RT) for 9 min. Tissue sections were then immunostained using p63α and cytokeratin 3 primary antibodies (Table 1). After fixation, sections were blocked with 5% normal goat serum and 0.25% Triton-X in PBS for 1 h at RT. Sections were then incubated with primary antibody overnight at 4 °C. After PBS washes, sections were stained with secondary Alexa Fluor 488 antibodies (Life Technologies, Paisley, UK) at a concentration of 1:500 for 1 h at RT. Nuclear counterstaining was then performed with propidium iodide in Vectashield® mounting medium (Vector Laboratories, Peterborough, UK) before addition of a coverslip for imaging using a Zeiss LSM 510 confocal microscope.

2.9. Wholemount immunochemistry of human limbal tissue and RAFT constructs

After 3 weeks in culture, cellular RAFT constructs were fixed for 30 min with 4% PFA. Human corneal tissue was fixed overnight at 4 °C in 4% PFA. The RAFT constructs were dissected into quarters and transferred to 48-well plates for staining with various antibodies (Table 1). Blocking and primary antibody steps were as section 2.8. The secondary antibody staining was combined with phalloidin staining (1:1000; Sigma–Aldrich Ltd., Dorset, UK) for 1 h at RT. RAFT pieces were transferred to slides, counterstained with DAPI in Vectashield® mounting medium and a coverslip added for imaging using a Zeiss 710 confocal microscope. Intact limbal tissue pieces were stained with phalloidin and propidium iodide alone, mounted and a coverslip secured using superglue for imaging on a Zeiss LSM 510 confocal microscope.

2.10. Histological staining of human limbal tissue and RAFT constructs

Cryosections of limbal tissue were fixed in 4% PFA for 9 min before being stained with haematoxylin and eosin (H and E) and a coverslip added with DPX. Sections were imaged using a Zeiss 510 microscope and Axiovision software. HLF cell counts were performed by counting cells in the stroma underlying the limbal crypts in an area of 200 × 500 μm (0.1 mm^2). A mean ± SD cell count per mm^2 was calculated from multiple tissue sections from triplicate donors. The resulting cell numbers led to the designation of optimal seeding densities for HLFs in RAFT constructs. RAFT constructs were embedded in paraffin and sectioned (5 μm) with a microtome. After rehydration through a series of alcohols to water, representative sections were stained with H and E, mounted and a coverslip added using DPX. Sections were imaged using a Zeiss LSM 510 confocal microscope and Axiovision software.

2.11. Scanning electron microscope imaging

Acellular RAFT constructs with BLCs were examined using scanning electron microscopy (SEM). Samples were fixed in Karnovsky's fixative, rinsed in cacodylate buffer and then post-fixed in osmium tetroxide before washing in distilled water and passing through a graded ethanol series. Samples were then critical point dried, mounted on stubs and splutter coated with gold before examination on a digital scanning variable pressure field emission SEM (Sigma, Carl Zeiss, Hertfordshire, UK).

2.12. Quantitative analysis of the characteristics of native crypts and BLCs

The surface topography of bioengineered RAFT constructs was analysed using H and E stained sections. Phalloidin and propidium iodide (PI) stained limbal tissue pieces were imaged using a Zeiss LSM 510 confocal microscope and Z-stack series were used to determine the size of cells within crypts and native crypt dimensions. Crypt depths were measured from the base of the crypts to the top of the stromal ridge, regardless of overlying epithelial layers. Depths and widths of native crypts and BLCs and cell area were measured using ImageJ software. Values are reported as mean ± SD. Student's *T*-test was used to determine significance ($p < 0.05$). Measurements were taken from triplicate RAFT constructs or biological specimens.

2.13. Putative stem cell marker, p63α, quantification in basal cells of BLCs on RAFT

In order to determine the number of cells in the base of BLCs expressing p63α, confocal Z-stack images of the base of crypts were analysed. This experiment was performed in triplicate with cells from three different donors. Three RAFT constructs per donor and 15 fields of view per construct were analysed. The percentage of DAPI stained nuclei also stained with p63α antibody was expressed as a mean ± SD.

3. Results

3.1. The human limbal epithelial stem cell niche

The corneal limbus, which is located at the junction between the transparent cornea and the conjunctiva (Fig. 1A), has been reported to be the primary location of LESCs. Anatomical stromal crypt structures have been identified that coincide with the Palisades of Vogt, which are especially visible in some intact corneas due to the abundance of melanocytes, seen here in a highly pigmented individual (Fig. 1B). Sectioning of fixed limbal tissue tangential to the central cornea and subsequent staining with H and E showed stromal protrusions, which create crypt-like structures allowing 12 or more cell layers to form in some regions (Fig. 1C). Abundant stromal cells were identified in close proximity to basal HLEs in the crypts and quantification using tissue sections revealed an average of 770 ± 160 cells/mm^2. A range of HLF seeding densities was tested in RAFT constructs in order to determine the optimal number to match approximately that seen in the native niche. Tissue sections of cellular RAFT were analysed and optimal seeding density was found to be 80,000 HLF/ml of collagen solution.

Immunochemical staining of native LC sections showed isolated cytokeratin 3 (CK3) expression, a marker of differentiated corneal epithelium, predominantly at the peripheral cornea and junction with the limbus and was most commonly restricted to the more superficial wing and squamous cells of the multilayered epithelium (Fig. 1D). Conversely, putative stem cell marker p63α, was expressed abundantly in the basal epithelial cells lining the base of the crypts (Fig. 1E). A series of confocal Z-stack images clearly revealed the decrease in cell size and change in morphology as optical sectioning moved from superficial, squamous epithelium, to the centre of crypts and finally to the basal epithelial cells that line the crypts (Fig. 1F). The basal images also highlighted the close proximity of stromal cells to the basal crypt cells. Quantification of epithelial cell size in different locations within crypts revealed that the cell area of HLEs lining the crypts was significantly smaller ($p < 0.001$) than that of cells located suprabasally within the centre of the crypt, 47.88 ± 12.82 μm^2 for basal crypt cells as opposed to 207.8 ± 37.25 μm^2 for suprabasal cells (Fig. 1G). The widths and depths of native crypts were measured using confocal Z-stack images and found to be varied, with average width of 107.9 ± 36.57 μm and average depth 68.9 ± 20.06 μm (Fig. 1H). Taken together, the evidence confirms that the smallest, p63α expressing cells, reside at the base of the limbal crypts and that underlying these basal epithelial cells is a population of stromal cells that are in close proximity.

3.2. Production of BLCs in RAFT constructs

The newly refined RAFT process involved the use of HPAs suitable for use in a conventional 24-well tissue culture plate. HPAs were placed on the surface of collagen hydrogels and incubated for a period of only 15 min on a plate heater set to 37 °C. During this

indicate movement through Z-stack from superficial epithelium to the base of LCs. Small arrows indicate stromal cells in close proximity to basal crypt cells. G) Representative orthogonal confocal image of human LCs used to determine basal and central crypt cell size. Arrows indicate basal cells lining crypts and stars indicate suprabasal cells. H) Average human LC dimensions (μm). Scale bars C, F, G 100 μm, D, E, 50 μm. (For interpretation of the references to colour in this figure legend, the reader is referred to the web version of this article.)

time, liquid was wicked from the hydrogel and absorbed by the HPAs. The HPAs were then removed and the resultant thin RAFT constructs remained attached to the base of the well plate, ready to receive a cell suspension on the surface (Fig. 2A). Using this process, it is possible to create micro-scale crypts on the surface of the RAFT constructs to mimic the 3-D physical structures of human LCs. In order to determine the correct specifications for the topology on the base of the HPAs, a mould tool was designed to produce a range of different sized protruding micro-ridges on the HPA surface. Each ridged HPA (RHPA) contained 4 sets of micro-ridges of equal widths and depths of either 100, 150, 200 or 250 μm surrounding a central flat area (Fig. 2B). A single RAFT construct displayed BLCs of different depths and widths dependent on the dimensions of the original micro-ridges on the RHPA (Fig. 2C). SEM images of the RHPAs show the porous nature of the material in addition to the uniformity in size of the micro-ridges (Fig. 2D). The simple RAFT process, which takes only 15 min, reliably created BLCs in the surface of the RAFT constructs, as seen with low and high magnification SEM imaging (Fig. 2D).

3.3. Characterisation of BLCs

OCT imaging was used to determine whether the overall thickness of the RAFT constructs was affected by the addition of the micro-ridges in the RHPAs. Average thickness after 3 weeks in culture was found to be 152.5 ± 9.19 μm in the HPA constructs (Fig. 3A) and 165.8 ± 9.61 μm in the RHPA created constructs (Fig. 3B). This difference was not found to be significant ($p > 0.05$). The BLCs were not visible in these images as it is difficult to discriminate between cells and collagen on the OCT images and the

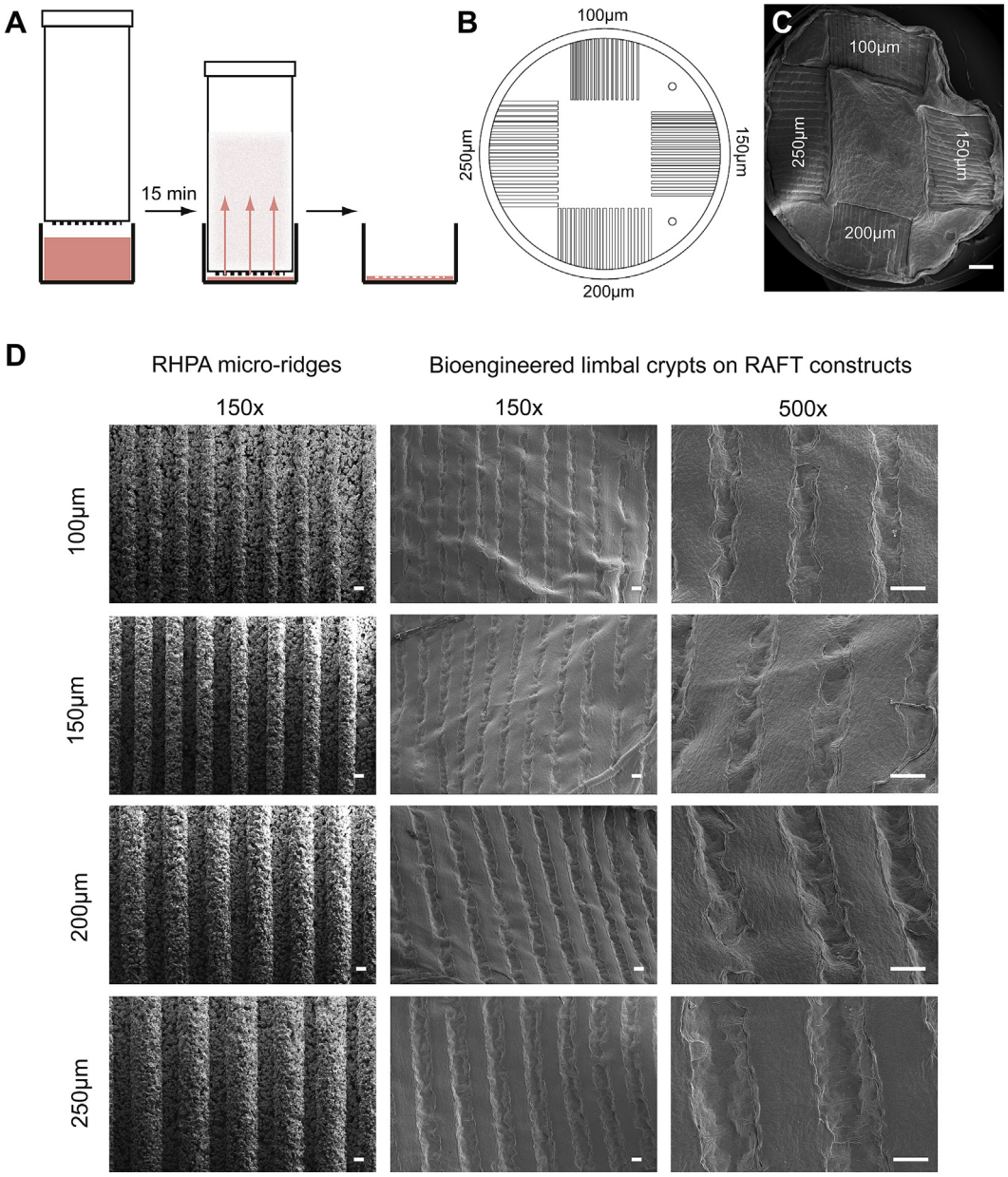

Fig. 2. Production of BLC-containing RAFT constructs using RHPAs. A) Schematic of the RAFT process using RHPAs. RHPAs are placed on top of a collagen hydrogel in a 24-well plate well and incubated for 15 min to allow wicking of liquid from the hydrogel. RHPAs are then removed and the RAFT construct remains at the bottom of the well. B) Schematic showing the pattern of topography of micro-ridges on the base of RHPAs. C) SEM images of a RAFT construct showing four different topologies on the same surface. D) SEM images of the protruding micro-ridges of variable depth on the RHPA surface and corresponding BLCs produced in the surface of the RAFT constructs. Scale bars C, 1 mm, D, 100 μm.

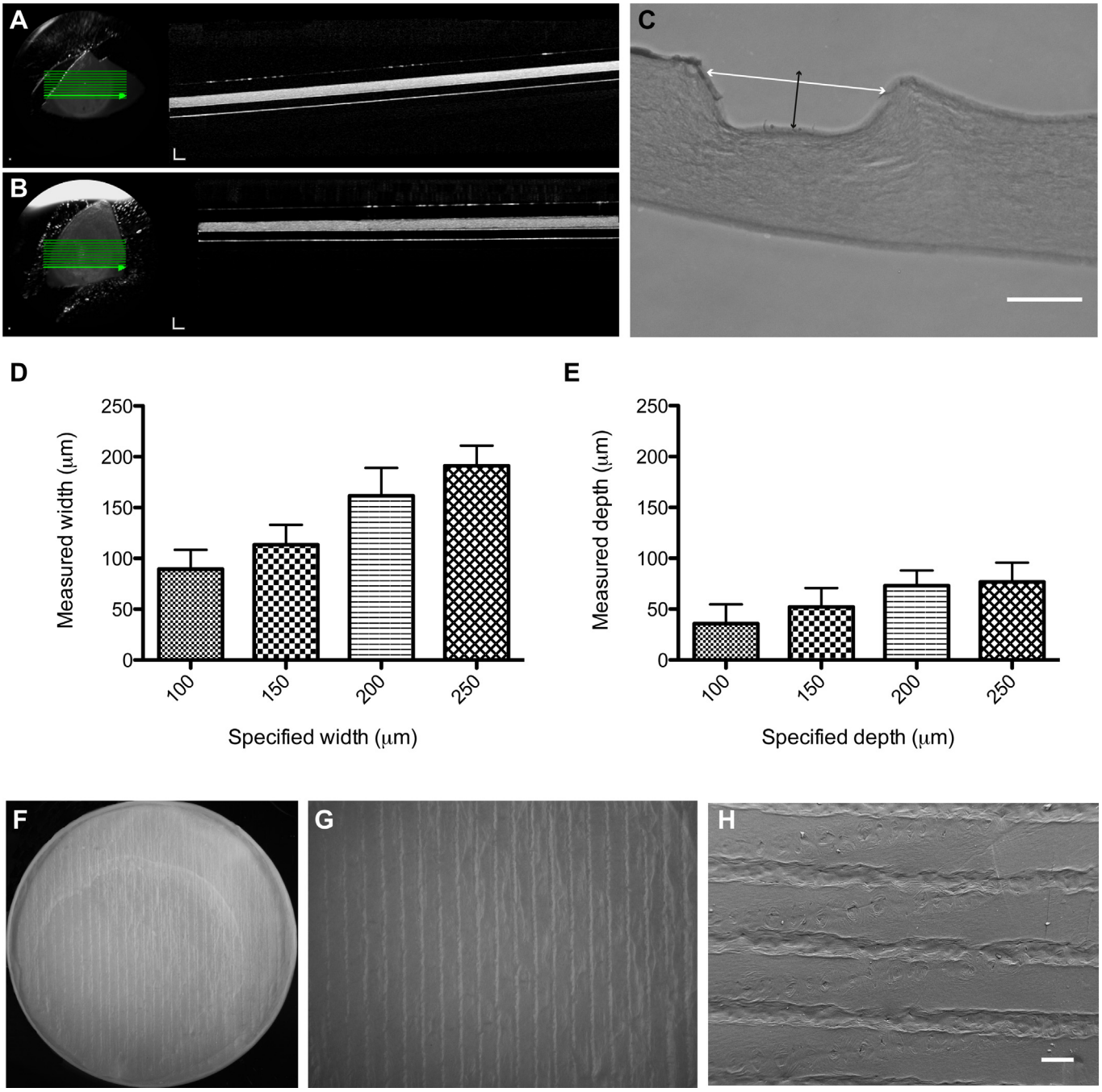

Fig. 3. BLCs in RAFT constructs. A) Representative OCT image of an unfixed RAFT construct produced using a HPA. B) Representative OCT image of an unfixed RAFT construct produced using a RHPA. C) Representative H and E stained section of a BLC on the surface of a RAFT construct. White arrow indicates width and black arrow depth measurements. D) Graph showing measured BLC widths in relation to micro-ridge width on RHPAs. E) Graph showing measured BLC depth in relation to micro-ridge depth on RHPAs. F) Whole RAFT construct with 175 μm BLCs. G) Higher magnification image of 175 μm BLCs with 250 μm spacing between crypts. H) SEM image of 175 μm BLCs. Scale bars A, B, H, 200 μm, C, 50 μm.

crypts are cell-filled. In order to determine the dimensions of the created BLCs, width and depth measurements of crypts were taken from transverse sections of paraffin embedded RAFT constructs (Fig. 3C). As the size of the micro-ridges in RHPAs increased, so did the width and depth of the created BLCs (Fig. 3D and E). The proportion of measured BLC width compared with micro-ridge width ranged from 75.7% to 89.4% whereas the measured depth compared with microridge depth was considerably lower at only, 30.7%–36.5% (Table 2). Based on these findings, to recreate a BLC of similar dimensions to the native crypts (approximately 70 μm deep and 110 μm wide) we chose to use 175 μm micro-ridges for further experiments. RHPAs with 175 μm micro-ridges covering the entire base were used to produce crypt-containing RAFT constructs in the same manner as previously stated. BLCs were created across the entire surface of the RAFT constructs in order to maximise the number of crypts available for analysis (Fig. 3F–H). Cells could then be seeded onto the surface of the RAFT constructs for cell culture.

3.4. Cell-filled BLCs

HCE-T cells were used to optimise cell seeding experiments on RAFT constructs with BLCs made using RHPAs. After 2 weeks in

Table 2
Measured widths and depths of BLCs compared to micro-ridge dimensions on RHPAs.

Micro-ridge dimensions (μm)	100	150	200	250
Mean measured width of BLCs (μm)	89.4 ± 18.98	113.5 ± 19.56	161.5 ± 27.53	191.1 ± 19.72
Proportion of micro-ridge width (%)	89.4	75.7	80.8	76.4
Mean measured depth of BLCs (μm)	35.8 ± 18.81	52.2 ± 18.45	73.0 ± 15.09	76.8 ± 18.87
Proportion of micro-ridge depth (%)	35.8	34.8	36.5	30.7

culture, histological sections indicated that cells formed an epithelium of approximately 3–4 cell layers on the flat regions of the RAFT construct. In areas with crypt topology this layering increased as cells filled the BLCs, forming multilayers approximately 5–7 cells deep (Fig. 4A). Confocal Z-stack images and orthogonal views highlighted the multilayering of cells as they filled the length of crypts (Fig. 4B). HLE cells formed a healthy, 3-4 cell multilayered epithelium on the flat surface of RAFT constructs containing HLFs. Where BLCs were present, the HLEs filled the crypts forming a multilayered epithelium of 6–7 cells in some regions (Fig. 4C). Confocal Z-stack images and orthogonal views indicated that cells filled the length of crypts and HLFs could be seen in close proximity to the cell-filled crypts in the underlying bioengineered collagen stroma (Fig. 4D). A series of confocal Z-stack images clearly highlighted the transition in cell size and cell morphology as the optical sections moved from superficial epithelium (0.0 μm from the surface) through to the base of a BLC (60.5 μm; Fig. 4E). The superficial epithelium was characterised by the presence of large, squamous epithelial cells with a low N/C ratio and lack of p63α expression. Deeper into the series, the cell-filled crypts became visible with HLFs in close proximity within the RAFT construct. The N/C ratio of cells at this level increased concomitantly with the expression of p63α, a putative stem cell marker, and high p63α expression was notable in cells lining the base of BLCs, with 79.2 ± 9.5% of basal crypt cells expressing p63α. A confocal line scan that optically sectioned a cell-filled crypt illustrated the presence of a multilayered epithelium and expression of p63α in the basal layers (Fig. 4F). Crypt containing RAFT constructs supported a mixed population of HLE cells indicated by immunochemical marker expression of a variety of proteins. Superficial HLEs expressed CK3 (Fig. 4G) and Pax6 (Fig. 4H), which is highly expressed in the cornea. In addition, cells filling crypts expressed proliferation marker, Ki67 (Fig. 4I).

4. Discussion

An investigation of the native limbal stem cell niche was essential to determine the specifications required for accurate recreation of the LCs. ImageJ analysis of stained wholemount corneas revealed LC depths and widths of approximately 70 μm and 110 μm, respectively. Others have attempted to assess the depth of the palisades of Vogt using a different method of *in vivo* confocal microscopy on healthy subjects and found an average depth of 120 μm but no width measurements were reported [18]. Their measurements would likely extend from palisade base to epithelial surface rather than stromal crypt peak as in our case, which may account for the difference. It has previously been reported that the smallest epithelial cells are located in the limbal basal epithelium [19] and we have confirmed that the basal epithelial cells of the crypts are the smallest in size. Small cell size and p63α expression are features that have been found to be indicative of increased clonal potential in epidermal keratinocytes and limbal epithelial cells [20,21]. Our evidence indicates that, as seen in the LGR5+ stem cells of the small intestinal crypts [22], LESCs are indeed located in a physically protective environment at the base of crypts. We have previously detailed the importance of replicating the close proximity of limbal stromal cells to limbal epithelial cells in a 3-D culture model [11]. Our one-step production process with RHPAs allows patterning of the surface while retaining viable HLFs in the body of the RAFT construct in close proximity to the basal HLEs. Additional niche cells could also be added to the bioengineered collagen stroma to further replicate the diverse mix of neighbouring cell types in this niche. This method produces a cell-populated, stable collagen construct that requires no further manipulation such as cell-lethal chemical crosslinking, an additional production step that would invariably increase manufacture time.

We have detailed a robust and rapid one-step method to produce surface topography on RAFT collagen constructs. The whole process, starting from creation of a cell-containing hydrogel to seeding of cells on the surface, only takes a maximum of 1.5 h with the actual crypt production process taking a rapid 15 min. This is in contrast to a previous example of an attempt to recreate artificial limbal micropockets. Ortega et al. use polyethylene glycol diacrylate (PEGDA), a synthetic polymer that is photocurable and can be crosslinked [23]. They are able to create micropockets of around 300 μm in diameter, but in order to render the material cytocompatible it requires washing for at least 4 days and to be functionalized with fibronectin to allow cell attachment. As we use type I collagen in our RAFT constructs, the most abundant collagen in the corneal stroma, it is immediately cytocompatible and there is no requirement to coat the surfaces for attachment. In fact, coating with fibronectin or laminin or a combination offers no additional benefit (data not shown). Bush and Pins combine photolithography, collagen processing and biochemical conjugation techniques to microfabricate crypts to mimic the dermal–epidermal junction [24]. They show successful multilayering of neonatal keratinocytes within the crypts but, again, their process was a lengthy multi-step process with different stages of production that required conjugation of fibronectin to the surface by carbodiimide 1-ethyl-3-(3-dimethylamionpropyl) carbodiimide hydrochloride (EDC). Furthermore, neither of these methods would allow seeding of supporting niche cells such as HLFs directly into the scaffold itself. Therefore, RAFT constructs may be considered to be more biomimetic.

Another advantage of the RAFT RHPA process is that the chosen pattern on the base of the HPAs is tunable to the needs of the end user. Micro-ridges can be made down to the order of tens of microns and there is no limit on the shape that is possible as the moulding process is very flexible. Consequently, this process could be transferable to numerous tissue-engineering applications where varied niche architectures are required. In addition, the nature of the biocompatible polymer absorber is such that limited particle shedding occurs during the absorption process, which is a critical factor for GMP compliance and future clinical applicability. The RAFT process also takes place in a standard format well plate allowing cells to be cultured on the surface directly after construct formation without the need to transfer to a different vessel. In our study, although highly reproducible, the measured depth of the BLCs did differ considerably from the specified depth of the RHPAs. This is most likely to be due to the creation of a dense fluid-leaving surface (FLS) in contact with the RHPA. There are a number of

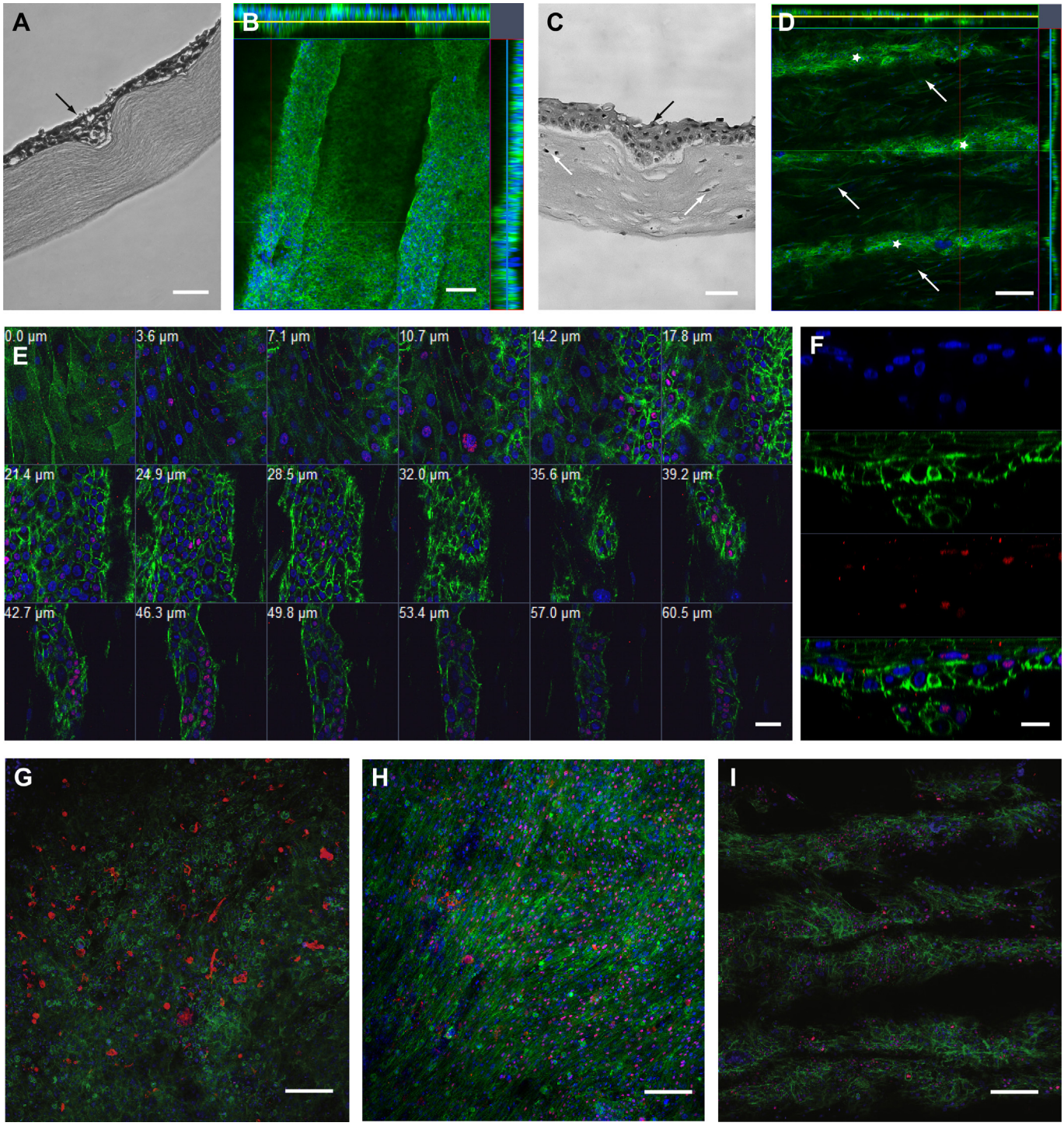

Fig. 4. Cell-filled BLCs. A) H and E stained paraffin embedded section of HCE-T cell filled BLCs (black arrow) on RAFT construct. B) Representative orthogonal confocal image of HCE-T cells in BLCs stained with phalloidin (green) and DAPI (blue). Yellow line indicates Z-stack position on *X*-axis and blue line on *Y*-axis. C) H and E stained paraffin embedded section of HLE cell filled BLCs (black arrow) on the surface of HLF (white arrow) containing RAFT constructs. D) Representative orthogonal confocal image of HLE cells in crypts (white stars) and HLF cells (white arrows) within the RAFT construct both stained with phalloidin (green) and DAPI (blue). Yellow line indicates Z-stack position on *X*-axis and blue line on *Y*-axis. E) Gallery view of a series of confocal Z-stack images showing an HLE cell filled BLCs and HLF cells within the RAFT construct stained with p63α (red), phalloidin (green) and DAPI (blue). Depth from the epithelial surface is indicated in μm on each image. F) Confocal line scan image of the HLE cell filled BLCs stained with p63α (red) phalloidin (green) and DAPI (blue). Confocal images of HLE cells on RAFT constructs with BLCs stained with G) CK3, H) Pax 6, I) Ki67 (red), phalloidin (green) and DAPI (blue). Scale bars A, C, 50 μm, B, G-I, 100 μm, D, 200 μm, E, 40 μm F, 20 μm. (For interpretation of the references to colour in this figure legend, the reader is referred to the web version of this article.)

reports describing the FLS acting as an ultra-filtration membrane leading to rapid accumulation of a layer of dense collagen fibrils at the surface [25–27], which could result in the specified depth becoming more of a challenge to obtain. However, one advantage of creating topology in the FLS is that the BLCs were stable over the time period we measured (3 weeks in culture) even with active cell-mediated matrix remodelling. This is perhaps not surprising as the RAFT process is known to involve a largely irreversible

deformation as fluid is removed from the collagen fibril network [27]. The introduction of BLCs to the RAFT constructs had no effect on the overall thickness of the constructs as indicated by OCT measurements and we have previously shown that RAFT constructs of similar thickness can be easily handled and sutured onto the surface of porcine eyes [16].

Our previous studies have shown that both corneal epithelial and corneal endothelial cells can be successfully cultured on the surface of RAFT constructs [11,16,28]. In the current study the BLC-containing RAFT constructs maintained a mixed population of primitive and more differentiated epithelial cells. Both the HCE-T cell line and primary HLEs filled the length of the crypts, and multilayered, which is the first time this has been shown with HLEs in BLCs. A high percentage of the cells lining the base of the crypts were found to be p63α positive, which is indicative of a stem cell phenotype and expressed in the basal cells of the native limbal niche. Multilayering of up to 7 layers in the crypt regions after 2 weeks submerged and only 1 week airlifting is a notable achievement with a limited number of superficial squamous cells showing expression of differentiated epithelial marker CK3 and Pax6, which is highly expressed in corneal epithelium. An abundance of Ki67 positive cells in the crypt-containing RAFT constructs indicated that cells do retain proliferative capacity on the BLC RAFT constructs. The stability of the BLCs over this time suggests that longer-term culture would be possible and could lead to an even greater number of multilayers.

The 3-D tissue architecture of the limbal crypts is one of several factors contributing to this stem cell niche. Here we have successfully incorporated two of those elements, the physical structure and the close proximity of the limbal fibroblasts. Further studies could introduce additional neighbouring cells, such as melanocytes or corneal stromal stem cells, to the collagen stroma, which would add yet another degree of biomimicry to this model of the limbal niche.

5. Conclusion

This study demonstrates the development of a rapid, one-step process to create cellular collagen constructs with BLCs to mimic the native LESC niche. The crypt making process takes a total of no more than 1.5 h from start to finish and takes into consideration GMP standards in the RAFT system materials and processes. A mixed population of HLEs can be maintained on the surface of RAFT constructs with a high percentage of p63α cells lining the crypts. RAFT provides an excellent *in vitro* model to study the behaviour of LESC by bio-mimicking both the close association of neighbouring niche cells in addition to the geometry of the 3-D microenvironment.

Acknowledgements

We would like to thank all the organ donors who donated their corneas for research. Thanks to Gordon Imlach from the Department of Materials Engineering at the Open University for his assistance with SEM imaging. Thanks to TAP Biosystems for the design and production of the HPA and custom RHPAs. This study was supported by the Technology Strategy Board, the EPSRC, and the National Institute for Health Research (NIHR) Biomedical Research Centre at Moorfields Eye Hospital NHS Foundation Trust and UCL Institute of Ophthalmology.

References

[1] Davanger M, Evensen A. Role of the pericorneal papillary structure in renewal of corneal epithelium. Nature 1971;229:560–1.
[2] Tseng SC. Regulation and clinical implications of corneal epithelial stem cells. Mol Biol Rep 1996;23:47–58.
[3] Schofield R. The relationship between the spleen colony-forming cell and the haemopoietic stem cell. Blood Cells 1978;4:7–25.
[4] Fuchs E, Tumbar T, Guasch G. Socializing with the neighbors: stem cells and their niche. Cell 2004;116:769–78.
[5] Theise ND, Saxena R, Portmann BC, Thung SN, Yee H, Chiriboga L, et al. The canals of hering and hepatic stem cells in humans. Hepatology 1999;30:1425–33.
[6] Schlötzer-Schrehardt U, Kruse FE. Identification and characterization of limbal stem cells. Exp Eye Res 2005;81:247–64.
[7] Shortt A, Secker G, Munro P, Khaw P, Tuft S, Daniels J. Characterization of the limbal epithelial stem cell niche: novel imaging techniques permit in vivo observation and targeted biopsy of limbal epithelial stem cells. Stem Cells 2007;25:1402–9.
[8] Ahmad S. Concise review: limbal stem cell deficiency, dysfunction, and distress. Stem Cells Transl Med 2012;1:110–5.
[9] Notara M, Shortt AJ, Galatowicz G, Calder V, Daniels JT. Il6 and the human limbal stem cell niche: a mediator of epithelial-stromal interaction. Stem Cell Res 2010;5:188–200.
[10] Mendez-Ferrer S, Michurina TV, Ferraro F, Mazloom AR, Macarthur BD, Lira SA, et al. Mesenchymal and haematopoietic stem cells form a unique bone marrow niche. Nature 2010;466:829–34.
[11] Levis HJ, Brown RA, Daniels JT. Plastic compressed collagen as a biomimetic substrate for human limbal epithelial cell culture. Biomaterials 2010;31:7726–37.
[12] Lutolf MP, Blau HM. Artificial stem cell niches. Adv Mater 2009;21:3255–68.
[13] Phillippi JA, Miller E, Weiss L, Huard J, Waggoner A, Campbell P. Microenvironments engineered by inkjet bioprinting spatially direct adult stem cells toward muscle- and bone-like subpopulations. Stem Cells 2008;26:127–34.
[14] Albrecht DR, Underhill GH, Wassermann TB, Sah RL, Bhatia SN. Probing the role of multicellular organization in three-dimensional microenvironments. Nat Methods 2006;3:369–75.
[15] Nelson CM, Tien J. Microstructured extracellular matrices in tissue engineering and development. Curr Opin Biotechnol 2006;17:518–23.
[16] Levis HJ, Menzel-Severing J, Drake RA, Daniels JT. Plastic compressed collagen constructs for ocular cell culture and transplantation: a new and improved technique of confined fluid loss. Curr Eye Res 2013;38:41–52.
[17] Araki-Sasaki K, Ohashi Y, Sasabe T, Hayashi K, Watanabe H, Tano Y, et al. An sv40-immortalized human corneal epithelial cell line and its characterization. Invest Ophthalmol Vis Sci 1995;36:614–21.
[18] Miri A, Al-Aqaba M, Otri AM, Fares U, Said DG, Faraj LA, et al. In vivo confocal microscopic features of normal limbus. Br J Ophthalmol 2012;96:530–6.
[19] Romano AC, Espana EM, Yoo SH, Budak MT, Wolosin JM, Tseng SCG. Different cell sizes in human limbal and central corneal basal epithelia measured by confocal microscopy and flow cytometry. Invest Ophthalmol Vis Sci 2003;44:5125–9.
[20] Barrandon Y, Green H. Cell size as a determinant of the clone-forming ability of human keratinocytes. Proc Natl Acad Sci U S A 1985;82:5390–4.
[21] Arpitha P, Prajna NV, Srinivasan M, Muthukkaruppan V. A subset of human limbal epithelial cells with greater nucleus-to-cytoplasm ratio expressing high levels of p63 possesses slow-cycling property. Cornea 2008;27:1164–70.
[22] Barker N, van Es JH, Kuipers J, Kujala P, van den Born M, Cozijnsen M, et al. Identification of stem cells in small intestine and colon by marker gene Lgr5. Nature 2007;449:1003–7.
[23] Ortega I, Deshpande P, Gill AA, Macneil S, Claeyssens F. Development of a microfabricated artificial limbus with micropockets for cell delivery to the cornea. Biofabrication 2013;5:025008.
[24] Bush KA, Pins GD. Development of microfabricated dermal epidermal regenerative matrices to evaluate the role of cellular microenvironments on epidermal morphogenesis. Tissue Eng Part A 2012;18:2343–53.
[25] Brown RA, Wiseman M, Chuo C, Cheema U, Nazhat SN. Ultrarapid engineering of biomimetic materials and tissues: fabrication of nano-and microstructures by plastic compression. Adv Funct Mater 2005;15:1762–70.
[26] Hadjipanayi E, Ananta M, Binkowski M, Streeter I, Lu Z, Cui ZF, et al. Mechanisms of structure generation during plastic compression of nanofibrillar collagen hydrogel scaffolds: towards engineering of collagen. J Tissue Eng Regen Med 2011;5:505–19.
[27] Alekseeva T, Hadjipanayi E, Abou Neel EA, Brown RA. Engineering stable topography in dense bio-mimetic 3D collagen scaffolds. Eur Cell Mater 2012;23:28–40.
[28] Levis HJ, Peh GS, Toh KP, Poh R, Shortt AJ, Drake RA, et al. Plastic compressed collagen as a novel carrier for expanded human corneal endothelial cells for transplantation. PLoS ONE 2012;7:e50993.